THE JOURNAL OF BIOLOGICAL CHEMISTRY VOL. 283, NO. 7, pp. 4004–4013, February 15, 2008

Serine 88 Phosphorylation of the 8-kDa Dynein Light Chain 1 Is a Molecular Switch for Its Dimerization Status and Functions*[S]

Received for publication, June 1, 2007, and in revised form, November 19, 2007 Published, JBC Papers in Press, December 4, 2007, DOI 10.1074/jbc.M704512200

Chunying Song[‡1], **Wenyu Wen**[§1], **Suresh K. Rayala**[‡1], **Mingzhi Chen**[¶], **Jianpeng Ma**[¶], **Mingjie Zhang**[§2], **and Rakesh Kumar**[‡‖3]

From the [‡]*Department of Molecular and Cellular Oncology, The University of Texas M.D. Anderson Cancer Center, Houston, Texas 77030, the* [§]*Department of Biochemistry, The Hong Kong University of Science and Technology, Clear Water Bay, Kowloon, Hong Kong, the* [¶]*Verna and Marrs McLean Department of Biochemistry and Molecular Biology and the* [‖]*Molecular and Cellular Biology, Baylor College of Medicine, Houston, Texas 77030*

Dynein light chain 1 (DLC1, also known as DYNLL1, LC8, and PIN), a ubiquitously expressed and highly conserved protein, participates in a variety of essential intracellular events. Transition of DLC1 between dimer and monomer forms might play a crucial role in its function. However, the molecular mechanism(s) that control the transition remain unknown. DLC1 phosphorylation on Ser^{88} by p21-activated kinase 1 (Pak1), a signaling nodule, promotes mammalian cell survival by regulating its interaction with Bim and the stability of Bim. Here we discovered that phosphorylation of Ser^{88}, which juxtapose each other at the interface of the DLC dimer, disrupts DLC1 dimer formation and consequently impairs its interaction with Bim. Overexpression of a Ser^{88} phosphorylation-inactive DLC1 mutant in mammary epithelium cells and in a transgenic animal model caused apoptosis and accelerated mammary gland involution, respectively, with increased Bim levels. Structural and biophysical studies suggested that phosphorylation-mimicking mutation leads to dissociation of the DLC1 dimer to a pure folded monomer. The phosphorylation-induced DLC1 monomer is incapable of binding to its substrate Bim. These findings reveal a previously unrecognized regulatory mechanism of DLC1 in which the Ser^{88} phosphorylation acts as a molecular switch for the transition of DLC1 from dimer to monomer, thereby modulating its interaction with substrates and consequently regulating the functions of DLC1.

Dyneins are massive minus-to-plus end microtubules motor complexes. Dyneins are categorized into axonemal dyneins and cytoplasmic dyneins on the basis of structural and functional features (1). Cytoplasmic dyneins are essential for a variety of fundamental intracellular events, such as organization and orientation of the mitotic spindle, nuclear migration, Golgi dynamics, retrograde neuronal axonal transport, and trafficking of vesicles and molecules (2–4). Dynein light chain 1 (DLC1)[4] (also known as DYNLL1, LC8, DLC8, and PIN), a ubiquitously expressed 89-amino acid protein, was initially identified as a light chain of the *Chlamydomonas* outer dynein arm (5). DLC1 is highly conserved from nematodes to mammals, and DLC1 orthologues share more than 90% sequence identity (6). DLC1 binds to a diverse array of proteins and RNAs, including neuronal nitric-oxide synthase (7), IκBα (8), p53-binding protein 1 (9), GKAP (10), gephyrin postsynaptic scaffolding proteins (11), Bim (12), Swallow (13), estrogen receptor (14), KIBRA (15), CDK2 (16), virus proteins (17, 18), parathyroid hormone mRNA (19), and possibly other proteins (20, 21).

Although DLC1 has been shown to bind to many partners, its physiological roles and the upstream regulators of DLC1 remain poorly understood. DLC1 is presumed to have essential cell functions because of its extraordinary sequence conservation across species and ubiquitous expression. Genetic studies in *Aspergillus* suggested that DLC1 is important for activities of dynein, because a DLC1 temperature-sensitive mutation led to multiple dynein-mediated defects (22). Several studies suggested that DLC1 might be critical for cell survival. Partial loss-of-function DLC1 alleles in *Drosophila* led to pleiotropic morphogenetic defects during development (23, 24). Complete deletion of DLC1 caused *Drosophila* embryonic lethality with excessive apoptosis. Studies from human cells and *in vitro* model systems have indicated a role of DLC1 in the cell survival pathways. For example, DLC1 prevented PC12 cells from undergoing apoptosis upon withdrawal of the neuronal growth factor by interaction and inactivation of neuronal nitric-oxide synthase (25). DLC1 also regulates apoptotic activities of Bim by sequestering it to the microtubule in certain cells. Upon apoptotic stimuli, Bim translocates jointly with DLC1 to the mitochondria and sequesters Bcl-2 from binding and inactivating Bak/Bax, thus allowing Bak/Bax to form an oligomer and initiate apoptosis (12).

* This work was supported in part by National Institutes of Health Grants CA80066 and CA90970 (to R. K.) and grants from the Research Grants Council of Hong Kong (to M. Z.). The costs of publication of this article were defrayed in part by the payment of page charges. This article must therefore be hereby marked "*advertisement*" in accordance with 18 U.S.C. Section 1734 solely to indicate this fact.

[S] The on-line version of this article (available at http://www.jbc.org) contains supplemental Figs. S1–S8.

[1] These authors contributed equally to this work.

[2] To whom correspondence may be addressed. E-mail: mzhang@ust.hk.

[3] To whom correspondence may be addressed. E-mail: rkumar@mdanderson.org.

[4] The abbreviations used are: DLC1, dynein light chain 1; Pak1, P21-activated kinase 1; RT, reverse transcriptase; MMTV, murine mammary tumor virus; STAT, signal transducers and activators of transcription.

Because of its protein structure and interaction with many apparently unrelated molecules, DLC1 has been thought to function as an adapter that links cargo proteins to the dynein motor (26). However, it may also function independently of dynein, as most of the DLC1 in the brain lysate does not bind to dynein (27). In addition to its potential role as a cargo adaptor of dynein, DLC1 was thought to have a role in promoting structure assembly and stabilization of complexes, such as IC74 and other dynein-unrelated complexes (28, 29). DLC1 binds to its target proteins by recognizing two different consensus peptide motifs: (K/R)*X*TQT and G(I/V)QVD (20, 30). X-ray diffraction and solution NMR structural studies have shown that DLC1 exists as a tight dimer consisting of two identical peptide-binding channels located at the opposite sides of the dimer interface (26, 31, 32). The structural properties of the DLC1 dimmer indicated that DLC1 might link dynein with target proteins to be transported by the motor. In addition, dimerization facilitates the interaction of DLC1 with its binding partners (26, 32). It has been shown that a change in pH drives the dimer-monomer transition due to protonation of His^{55} buried in the dimer interface, and His^{55} protonation occurs at pH 4.5 or below (33). It has been suggested that the dimmer to monomer transition might play a regulatory role in the function of DLC1 (33).

Phosphorylation is a key post-translational modification that regulates many aspects of the cellular signaling pathways. Previous studies showed that DLC1 is phosphorylated on Ser^{88} by p21-activated kinase 1 (Pak1), a major signaling nodule in mammalian cells (34). DLC1 phosphorylation by Pak1 promotes the survival and anchorage-independent growth of breast cancer cells. Interestingly, DLC1-Ser^{88} phosphorylation by Pak1 also regulates the interaction of DLC1 with Bim, and such events are accompanied by the release of Bim from the DLC1-Bim complex and degradation of Bim. Pak1 phosphorylation of DLC1 at Ser^{88} also controls DLC1-trigged macropinocytosis (35). All these studies indicate that Ser^{88} phosphorylation of DLC1 represents an important convergence point for upstream signals. In the present study, we explored the potential modulating effect of Ser^{88} phosphorylation upon DLC1 and its effect on the function of DLC1.

EXPERIMENTAL PROCEDURES

Model Preparation—The initial coordinates were taken from the solution structure of DLC1 from the Brookhaven Protein Data bank (PDB code 1F3C). The wild-type models of various dimer combinations of DLC1 were generated by keeping the initial backbone coordinates of the point mutations, and the side chain coordinates were then generated using the CHARMM program. The missing hydrogen coordinates were built with the HBUILD algorithm. To get a suitable conformation of the modeled parts, we first put each protein model into the pre-generated octahedral water box; then, depending on the charging status, counterions were added to neutralize the system. After that, we performed a total of 700 steps of steepest descent energy minimization with PMEwald and periodical boundary conditions, gradually releasing the system every 100 steps by reducing the harmonic anchor from 100.0 to zero for proteins, modeled side chains, and the rest.

Graphic Illustration—After the minimizations, the models were in more suitable conformations. We used MOLSCRIPT to make cartoons for models and controls. The electrostatic surface of each model was prepared by GRASP.

Expression Vectors and Cloning—pcDNA3.1 vectors (Invitrogen) containing human DLC1, DLC1-S88A, or DLC1-S88E cDNA were previously reported (34). In the original cloning from the mammary gland cDNA library, the DLC1 cDNA contained the coding region as well as 48 base pairs of 5′-untranslated region; thus translation of this expression vector resulted in a protein with an apparent molecular mass of 16 kDa. However, this region had no effect on the functions and activities of DLC1. Subsequently generated DLC1-S88A or DLC1-S88E cDNA lacked this untranslated region, and each had an apparent molecular mass of 15 kDa. To demonstrate a lack of any effect of this 48-bp region in the original cloning, we generated a new T7-DLC1 construct with only DLC1 cDNA (T7-DLC1-new) and tested whether this construct behaved the same as T7-DLC1, using the immunoprecipitation assay. The result showed that T7-DLC1-new had the same ability to interact with endogenous DLC1, and this excluded the possibility of the interference of extra untranslated region in T7-DLC1 (supplementary Fig. S1).

Cell Culture and Plasmid Transfection—Transient transfections were performed using a FuGENE-6 kit (Roche Applies Science) in accordance with the manufacturer's instructions. HC11 mammary epithelial cells were grown in RPMI 1640 medium (Cell Signaling) containing 2 mM L-glutamine, 1× antibiotic/antimycotic solution, 5 μg/ml bovine insulin (Sigma), 10 ng/ml mouse epidermal growth factor (Sigma), and 10% fetal bovine serum. HC11 cells stably expressing DLC1 were generated by transfecting pcDNA3.1, pcDNA-T7-DLC1, or pcDNA-T7-DLC1-S88A plasmids using electroporation. To obtain apoptotic cells, cells were allowed to attach for 24 h in medium without insulin or epidermal growth factor, reaching about 80% confluence. Then, the cells were cultured in serum-free medium without insulin and epidermal growth factor for the times indicated under "Results."

Pak1 Kinase Assay—For stimulation of Pak1 kinase activity by spingosine, 8 h after transfection with T7-DLC1 cDNA plasmids, the 293T cells were serum starved for 36 h and then treated with sphingosine (100 μM) for 15 and 30 min. Part of the whole cellular lysate was used for the Pak1 kinase assay as described previously (34). We analyzed the reaction products by SDS-PAGE and autoradiography. The same blot was then used for examining the immunoprecipitation result by Western blotting for Pak1.

Annexin V and TUNEL Assays—The Annexin V assay was conducted with an Annexin V-fluorescein 5-isothiocyanate apoptosis detection kit (Sigma). Cells were induced to undergo apoptosis by withdrawal of serum and other survival factors from the medium for 24 h, and the assay was then performed according to the manufacturer's instructions. The TUNEL assay was performed by using the fluorescein In Situ Cell Death Detection kit (Roche Diagnostics) according to the manufacturer's instructions. One thousand cells from five random fields per section were documented by photomicroscopy, and the TUNEL-positive epithelial cells were counted.

Generation of MMTV-DLC1 and MMTV-DLC1-S88A Transgenic Mice and DNA Analysis—To express the transgenes in the mouse mammary glands, the cDNAs encoding human DLC1 and DLC1-S88A with the T7 tag were subcloned from the pcDNA3.1 vector into the MMTV-SV40-BssK vector using sites HindIII-XbaI (blunted) into HindIII-EcoRI (blunted). The transgenes were excised from plasmid DNA by restriction enzymes SalI and SpeI, and the resulting linear fragments contained promoter sequences, DLC1 or DLC1-S88A coding regions, and 3′-untranslated regions and SV40 polyadenylation signals. The linear DNA fragments were microinjected into the pronuclei of the B6D2F1/J hybrid mouse eggs. Genotyping was performed by using the polymerase chain reaction assay. The primers used were forward primer to the T7-epitope encoding region (5′-CAGCAAATGGGTCGGGATC) and reverse primer (5′-CTACCGAAGTTCCTCCCCAC) corresponding to DLC1 cDNA. Genotyping was confirmed by Southern blot analysis of mouse tail genomic DNA digested with HindIII and SpeI restriction enzymes. The probe used was full-length DLC1 cDNA, which was digested out from a plasmid named RFP-PINS88A containing cDNA of DLC1 (previously generated in the laboratory) by restriction enzyme EcoRI plus XhoI.

Mouse Husbandry and Analysis Strategies—The mice were maintained on a mixed C57/BL6:DBA background. For analysis of the mouse mammary gland development, mammary tissues from involution days 1 to 5 (first pregnancy with forced involution after day 10 of lactation) were analyzed. Age-matched wild-type mice served as controls in these studies.

RT-PCR Analysis—The RNAs were treated with DNase I to eliminate potential DNA contamination using the DNA-free kit (Ambion) according to the manufacturer's instructions. RT-PCR was performed using the Access Quick RT-PCR system (Promega). Primers for DLC1 and DLC1-S88A were the same as for PCR of DNA. Mouse glyceraldehyde-3-phosphate dehydrogenase was used as internal control with primers forward, 5′-CCATCTTCCAGGAGCGAGATC, and reverse, 5′-CGTTCAGCTCAGGGATGACC. Primers for mouse Bim total were forward, 5′-CTGTTGGATCCACCATGGCCAAGCAACCT, and reverse, 5′-TGCATGTGCGGCCGCTCAATGCCTTCTC. Mouse β-actin primers were forward 5′-TTTGATGTCACGCACGATTTCC, and reverse, 5′-TCTACGAGGGCTATGCTCTCC.

Immunoblot and Immunoprecipitation Analysis—About 50 μg of total protein extract from cultured cells or mammary glands was used in the immunoblot assays. The lysates to immunoprecipitate T7-tagged proteins were immunoprecipitated for 2 h at 4 °C using 50 μl of T7-agarose beads per milligram of protein. The antibodies used and the dilutions were as follows: mouse T7 tag (1:5000, Novagen), rabbit polyclonal BCL-X(L) (1:1000; Santa Cruz Biotechnology), rabbit polyclonal Bim (1:500; Stressgen), rabbit polyclonal Stat3 serine 705 phosphorylation (1:1000; Cell Signaling), mouse monoclonal total Stat3 (1:500; Cell Signaling), and mouse monoclonal β-actin (1:1000; Sigma).

Immunohistochemical Analysis—The sections were incubated with polyclonal rat Bim antibody (1:50; Chemicon) at 4 °C overnight and horseradish peroxidase-conjugated anti-rat secondary antibody (1:200). Immunostained sections were lightly counterstained in hematoxylin with submerging into hematoxylin. Immunostaining for T7 was performed as reported previously (34).

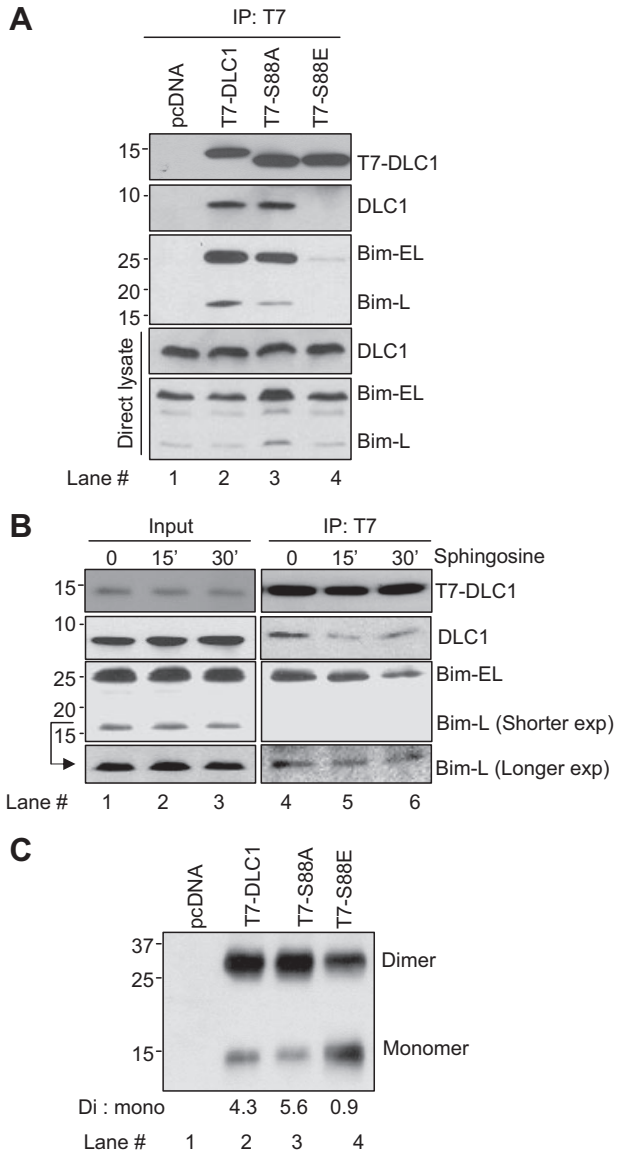

FIGURE 1. **DLC1-Ser[88] phosphorylation mutants modulate its interaction with endogenous DLC1 and dimerization.** *A*, total cellular lysates from 293T cells transfected with pcDNA, T7-tagged DLC1, S88A, and S88E were immunoprecipitated (*IP*) with T7 antibody, followed by Western blot analysis for DLC1 and Bim. The DLC1 antibody was able to detect both T7-tagged and endogenous DLC1. Direct lysate lanes are shown in the *lower panels*. *B*, effect of sphingosine signaling on T7-DLC1 interaction with endogenous DLC1 and Bim. After 8 h of transfection, the 293T cells were serum starved for 36 h and then treated with sphingosine (100 μM) for 15 and 30 min. The whole cellular lysates were used for the immunoprecipitation assay as in *A*. The *arrow* points to a longer exposure for the Bim-L protein band. *C*, 293T cells transfected with pcDNA, T7-tagged DLC1, S88A, and S88E were chemically cross-linked with disuccinimidyl suberate (3 μM), followed by Western blot analysis with T7 antibody. The results shown are representative of three separate experiments.

Statistical Analysis and Quantification—Results are expressed as mean ± S.E. Statistical analysis of the data were performed using Student's *t* test. Blots were quantified with ImageQuant software.

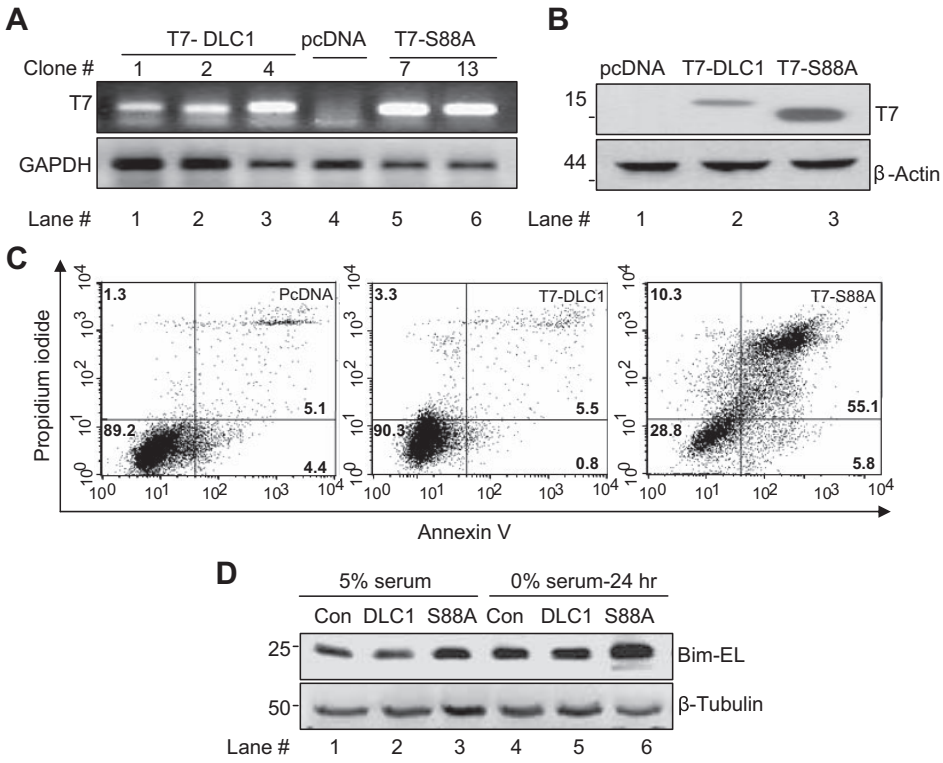

FIGURE 2. **DLC1-S88A promotes apoptosis and increases Bim protein level.** *A*, RT-PCR analysis showing expression of T7-tagged DLC1 and DLC1-S88A in HC11 clones. RT-PCR amplified exogenous DLC1 or DLC1-S88A only, not the endogenous DLC1. *B*, the clones were pooled together and expression of the transfected plasmids was analyzed by Western blotting with T7 antibody. *β*-Actin was used as an internal control. *C*, Annexin V staining assay of HC11/pcDNA, HC11/T7-DLC1, and HC11/T7-S88A cells growing in medium without survival factors for 24 h. *D*, Western blot analysis of Bim protein level of HC11/pcDNA, HC11/T7-DLC1, and HC11/T7-S88A cells growing in medium with or without survival factors. All these experiments were performed three times. *GAPDH*, glyceraldehyde-3-phosphate dehydrogenase.

NMR Studies—Preparation of the wild-type DLC1 and its S88A and S88E mutants followed the procedure described in our earlier work (26). ^{1}H-^{15}N HSQC spectra of ^{15}N-labeled DLC1 and its S88A and S88E mutants were acquired on a Varian Inova 750-MHz spectrometer equipped with a *z*-gradient shielded triple resonance probe. All NMR spectra were recorded at 30 °C, with a protein concentration of ~0.3 mM dissolved in 100 mM potassium phosphate buffer, pH 3.0 or 6.0.

Gel Filtration Chromatography—Analytical gel filtration chromatography was performed on an AKTA FPLC system using a Superose 12 10/30 column (Amersham Biosciences). Protein samples were dissolved in 20 mM Tris-HCl buffer, pH 7.5, containing 1 mM EDTA, 1 mM dithiothreitol, and 100 mM NaCl. The column was calibrated with the low molecular mass column calibration kit from Amersham Biosciences.

Fluorescence Assays—The 9-residue peptide (MSCDK-STQT) corresponding to Met[48] to Ser[56] of Bim was commercially synthesized (GenScript) and was >95% pure. The fluorescence polarization assays were performed on a PerkinElmer LS-55 fluorimeter equipped with an automated polarizer at 20 °C. The peptide was conjugated with fluorescein 5-isothiocyanate (Invitrogen) on its N-terminal amine. Fluorescence titration was performed with an increasing amount of unlabeled DLC1 proteins and a constant amount of fluorescein 5-isothiocyanate-labeled peptide (1 μM) in 20 mM Tris-HCl buffer, pH 7.5, containing 1 mM EDTA, 1 mM dithiothreitol, and 100 mM NaCl. The titration curves were fitted with the MicroCal Origin software package.

RESULTS AND DISCUSSION

DLC1-Ser[88] Phosphorylation Mutants Modulate Its Interaction with Endogenous DLC1 and Dimerization—Although a previous *in vitro* study (34) using recombinant proteins demonstrated that phosphorylated DLC1 or DLC1-S88E mutant (phosphorylation mimicking mutation) abolished the interaction of DLC1 with Bim, whereas there was no effect of the DLC1-S88A mutant (phosphorylation inactive mutation) on its *in vitro* binding to Bim, the nature of such interactions in a cellular *in vivo* setting remains to be verified. In addition, *in vivo* phosphorylation of DLC1 on Ser[88] has been shown to be accompanied by degradation of Bim (34). To gain a deeper understanding of the potential effect of DLC1-Ser[88] phosphorylation on the structure of DLC1, we first constructed the three-dimensional models *in silico*. Using the coordinates from the solution structure of the DLC1 dimer (PDB code 1F3C), we modeled the following DLC1 dimers: DLC1 homodimer (supplementary Fig. S2A), DLC1 homodimer with phosphorylated Ser[88] (supplementary Fig. S2B), DLC1-S88E homodimer (supplementary Fig. S2C), DLC1-S88A homodimer (supplementary Fig. S2D), and DLC1 heterodimer with DLC1-S88A mutant (supplementary Fig. S2E). The calculations of electrostatic surface potential for each model showed that the introduction of phosphorylation or glutamic acid on Ser[88] dramatically intensified the negative electrostatic charges around the edge of the dimer interface; in contrast, a comparatively low surface negative charge was shown in dimers consisting of DLC1-S88A or DLC1/DLC1-S88A. Because Ser[88] from the two subunits juxtapose each other at the interface of the DLC dimer, the introduction of the negative charges in the proximity of Ser[88] is expected to reduce the stability of the DLC8 dimer.

To test the prediction that Ser[88] phosphorylation may impair the interaction between the two subunits in the DLC1 dimer, we examined the ability of transiently transfected T7-DLC1 or its S88A or S88E mutant to interact with the endogenous DLC1 or its substrate Bim in 293T cells. Immunoprecipitation of cell lysates with anti-T7-agarose beads revealed the inability of T7-DLC1-S88E to pull-down the endogenous DLC1 or Bim, compared with the efficient interactions of T7-DLC1 or T7-DLC1-S88A with DLC1 or Bim (Fig. 1*A* and supplementary Fig. S3). These results suggested that DLC1-Ser[88] phosphorylation mimicking active mutant inhibits its interaction with the

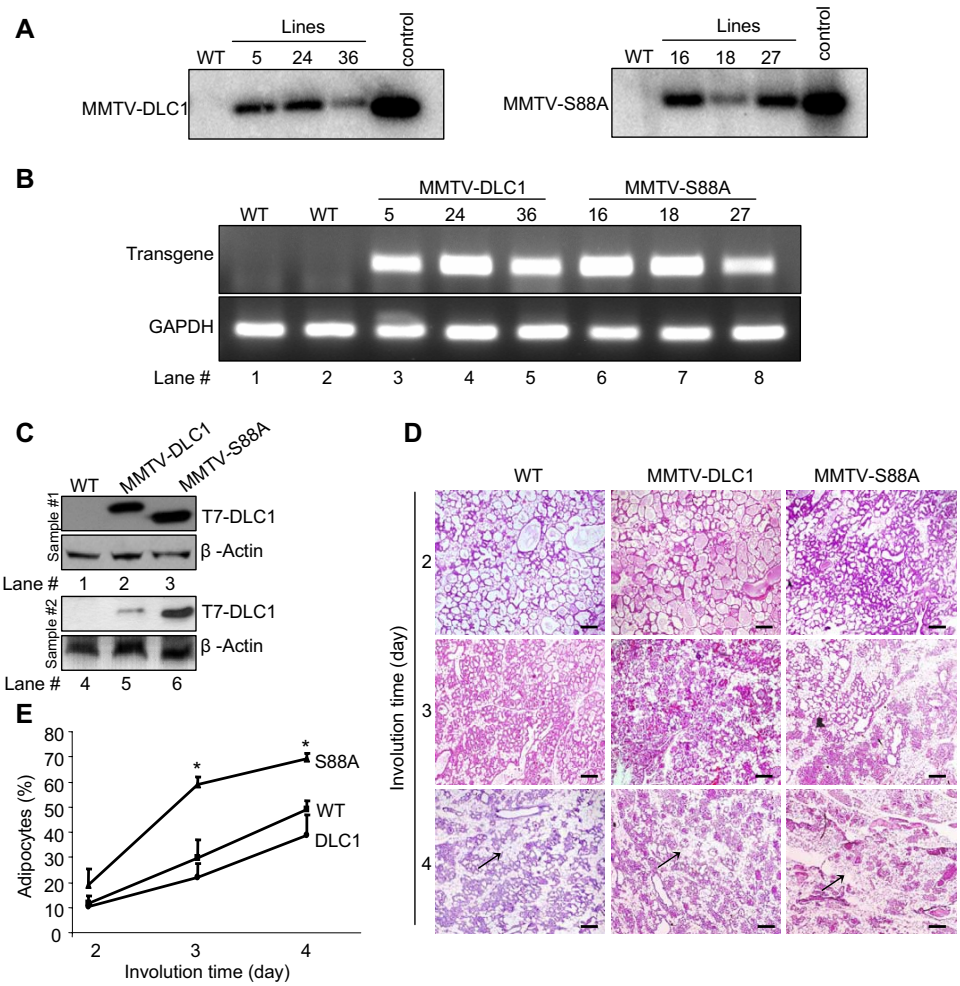

FIGURE 3. **Mammary glands from MMTV-S88A mice showing faster mammary involution.** *A*, Southern blot detection of the transgene in the mouse tail genomic DNA. About 10 μg of DNA per mouse sample was digested with HindIII and SpeI restriction enzymes. About 10 ng of plasmid DNA creating the transgenic animals were digested together with genomic DNA for use as positive controls. *B*, transgene mRNA level expression in the mammary glands detected by reverse transcriptase-polymerase chain reaction. *C*, transgene protein expression in the mammary glands was detected by T7 immunoprecipitation (*IP*) followed by Western blotting of T7 antibody. Input lanes show actin as a loading control. *D*, MMTV-S88A mice showing faster mammary involution. The mammary involution was initiated by removing the pups on lactation day 10. Representative hemotoxylin and eosin staining of mammary glands from wild-type (*WT*), MMTV-DLC1, and MMTV-S88A mice during involution at days 2, 3, and 4 are shown. *Bars*, 200 μm. *Arrows* show adipocytes. *E*, quantification of adipocyte content of WT, MMTV-DLC1, and MMTV-S88A mammary glands during involution from the indicated time points (three mice per time point). The values are expressed as the percentage of the area filled with adipocytes in five randomly selected fields in the mammary gland. The values of MMTV-DLC1 mouse or MMTV-S88A mouse mammary glands *versus* WT glands were analyzed by Student's *t* test (*, $p < 0.05$). Results shown are representative of three individual experiments. *GAPDH*, glyceraldehyde-3-phosphate dehydrogenase.

endogenous DLC1 as well as with Bim. To validate these results, we next examined the effect of DLC1-Ser^{88} phosphorylation on its binding to DLC1 and Bim by a physiologic signal sphingosine, a known Pak1 activator (36). 293T cells transfected with T7-DLC1 were stimulated by sphingosine to activate Pak1, and cell lysates were immunoprecipitated with an anti-T7-monoclonal antibody and blotted with anti-DLC1 and Bim antibodies. Upon Pak1 activation by sphingosine (supplementary Fig. S4), there was a significant reduction in the ability of T7-DLC1 to interact with endogenous DLC1 or Bim-EL/Bim-L (Fig. 1*B*).

To demonstrate the existence of DLC1 dimer and examine the effect of Ser^{88} phosphorylation on DLC1 dimerization, 293T cells transfected with T7-DLC1 or its Ser^{88} phosphorylation mutants were chemically cross-linked with disuccinimidyl suberate, and the cell lysates were immunoblotted with anti-T7-monoclonal antibody. In addition to the monomer forms of T7-DLC1 proteins, which migrated with an apparent molecular mass of 15 kDa, the immunoblot analysis indicated the existence of a 30-kDa T7-DLC1 dimer as expected (Fig. 1*C*). The immunoblot analysis also showed a clear decrease of the T7-S88E dimer-to-monomer ratio (0.9-fold) compared with the dimer-to-monomer ratio (4.3-fold) of T7-DLC1 or T7-S88A (5.6-fold) (Fig. 1*C*). Taken together, these findings suggested that Ser^{88} phosphorylation diminishes the ability of DLC1 to form a dimer.

DLC1-Ser^{88} Phosphorylation-inactive Mutant Enhances Apoptosis in a Cellular Model—DLC1 has been shown to exert a survival function in *Drosophila* embryonic development (23, 24) and in human neuronal cells (25). Furthermore, DLC1 protein levels were down-regulated in HC11 mammary epithelium cells upon apoptosis (37), implying a putative role of DLC1 in supporting cell survival. To better understand the functional significance of Ser^{88} phosphorylation on the function of DLC1, we examined the effect of the phosphorylation-inactive DLC1-S88A mutant on the survival of HC11 cells. We generated HC11 clones stably expressing T7-DLC1, DLC1-S88A, and control vector as assessed by RT-PCR (Fig. 2*A*) and Western blotting (Fig. 2*B*). To examine the potential effect of DLC1-S88A on cell survival, HC11 clones were subjected to serum deprivation for 24 h, and the status of cellular apoptosis was assayed using the Annexin V staining assay. Under normal culturing conditions, no apoptotic cells could be detected in any of the clones. However, upon serum starvation, about 50% of the HC11/DLC1-S88A cells underwent apoptosis. In contrast, only 5% of the HC11/DLC1 cells or HC11/pcDNA cells underwent apoptosis (Fig. 2*C*). These observations indicated that inactivation of Ser^{88} phosphorylation impairs the cell survival activity of DLC1 in the cultured cells.

DLC1-Ser^{88} phosphorylation has been shown to be accompanied by the release of Bim from the DLC1-Bim complex,

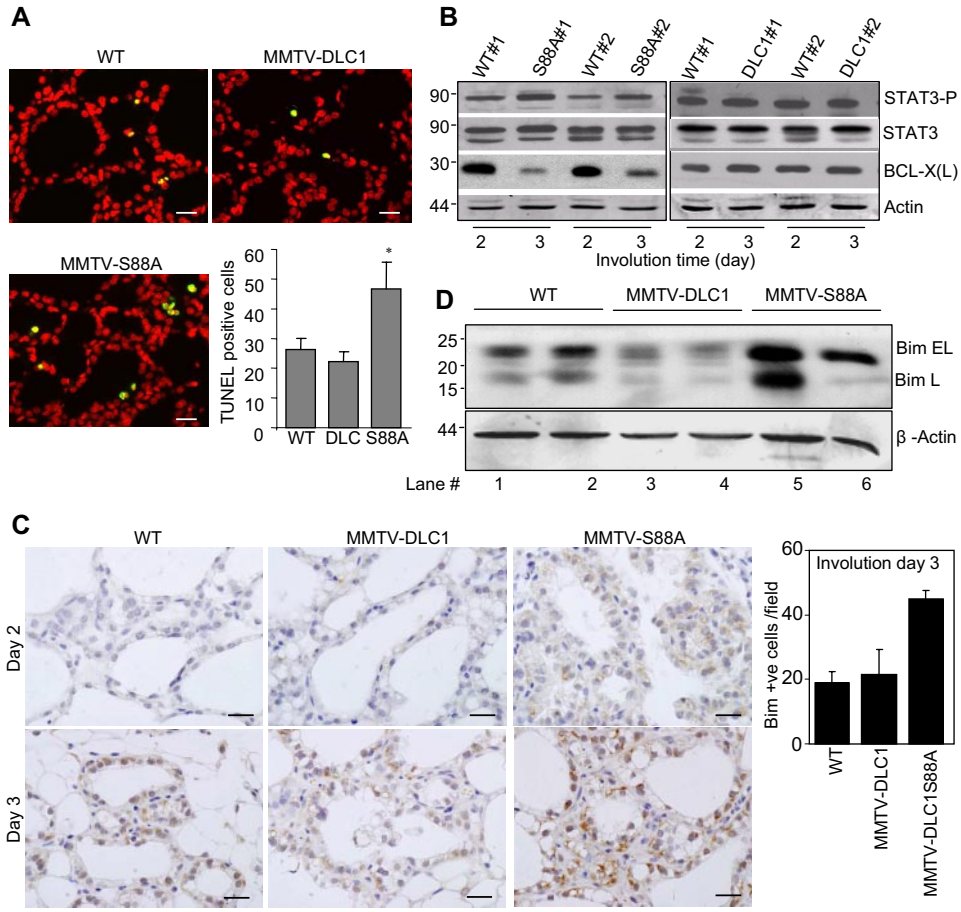

FIGURE 4. **Mammary glands from MMTV-S88A mice showing more apoptosis and increased Bim.** *A*, terminal deoxynucleotidyl transferase biotin-dUTP nick end labeling (TUNEL) staining of involution day 3 mammary glands from wild-type (*WT*), MMTV-DLC1, and MMTV-S88A mice. *Red*, 4′,6-diamidino-2-phenylindole; *green*, fluorescein 5-isothiocyanate-labeled dUTP incorporated into fragmented DNA by transferase. *Bars*, 50 μm. Quantification of apoptotic cells (three mice per time point): the numbers of TUNEL-positive cells of 1000 cells from five randomly selected fields were used as apoptotic values. The values of MMTV-DLC1 mouse or MMTV-S88A mouse mammary glands *versus* WT glands were analyzed by Student's *t* test (*, $p < 0.05$). *B*, protein level of STAT3-Thr^{705} phosphorylation, total STAT3, Bcl-xL, and actin of involution days 2 and 3 mammary glands from WT, MMTV-DLC1, and MMTV-S88A mice examined by Western blotting. *C*, immunohistochemical assay of Bim protein level in mammary glands at days 2 and 3 involution from WT, MMTV-DLC1, and MMTV-S88A mice. Bim-positive cells are in *brown*. *Bar graphs* show quantification of Bim-positive cells in a given field at involution day 3. *D*, Western blot assay of Bim protein level in mammary glands at day 3 involution from WT, MMTV-DLC1, and MMTV-S88A mice. Results shown are representative of three individual experiments.

thereby promoting degradation of Bim and inhibition of apoptosis (34). It is predicted that stabilization of the DLC1 dimer by the S88A mutation would lead to stabilization of Bim. To test this hypothesis, we assayed the cellular Bim level in S88A cells. Although there was no difference at the RNA level (supplementary Fig. S5), Western blot analysis showed a clear increase of Bim protein in the HC11/DLC1-S88A cells after serum starvation compared with the level of the protein in the HC11/DLC1 or control cells (Fig. 2*D* and supplementary Fig. S6). Although the Bim antibody used here (Stressgen) is able to recognize all three Bim isoforms (EL, L, and S), we detected only the EL form in our experiments, probably due to no or very low levels of L and S isoforms in HC11 cells. These findings suggested that overexpression of a phosphorylation-inactive mutant of DLC1 promotes apoptosis due to an increase of the cellular Bim protein level.

DLC1-Ser^{88} Phosphorylation-inactive Mutant Mice Exhibit Accelerated Mammary Involution and an Increase of Apoptosis—To study the role of DLC1-Ser^{88} phosphorylation in a more physiologic whole animal setting, we created transgenic mouse lines overexpressing T7-DLC1 or T7-DLC1-S88A in the mammary epithelium. Full-length tagged cDNAs of the wild-type or S88A mutant were placed under the MMTV promoter and microinjected into B6D2F1/J mouse embryos. Founders with integration of the transgene constructs into the genome were screened with PCR and confirmed by Southern blot analysis. A total of three lines of each transgenic mouse were established, with lines 5, 24, and 36 for MMTV-DLC1 mice and lines 16, 18, and 27 for MMTV-DLC1-S88A mice (Fig. 3*A*). These mouse lines expressed the transgenes at the RNA level (Fig. 3*B*). The protein level of the transgene was detected by immunoprecipitation using anti-T7 antibody followed by immunoblotting with a T7-monoclonal antibody (Fig. 3*C*). We proceeded to evaluate the effect of the DLC1-S88A mutant on the apoptosis during involution in DLC1-TG (lines 5 and 24) and DLC1-S88A-TG (lines 18 and 27) lines. The selection of lines was based on transgene expression.

We next studied the mammary gland involution in the MMTV-DLC1, MMTV-DLC1-S88A, and control mice by removing the pups after 10 days of lactation to initiate the process of involution. The number 4 inguinal mammary glands from involution time days 1 to 4 were dissected and analyzed by hemotoxylin and eosin staining. Until day 1 of involution, the mammary glands exhibited expanded alveoli that were surrounded with single-layered epithelial cells. On involution day 2, alveoli of the mammary glands started to regress, and adipocyte cells began to repopulate. This process was more distinct in mammary glands from the MMTV-S88A mice (Fig. 3*D*). On involution day 3, the majority of lobuloalveolar structures collapsed and formed clusters of epithelial cords with small lumina. Ducts appeared and fat cells were obvious. Mammary glands from MMTV-DLC1 mice showed a phenotype similar to that of the wild-type mice, whereas mammary glands from MMTV-S88A mice had accelerated involution progression until day 4, with the regression of the epithelial component and re-emergence of adipo-

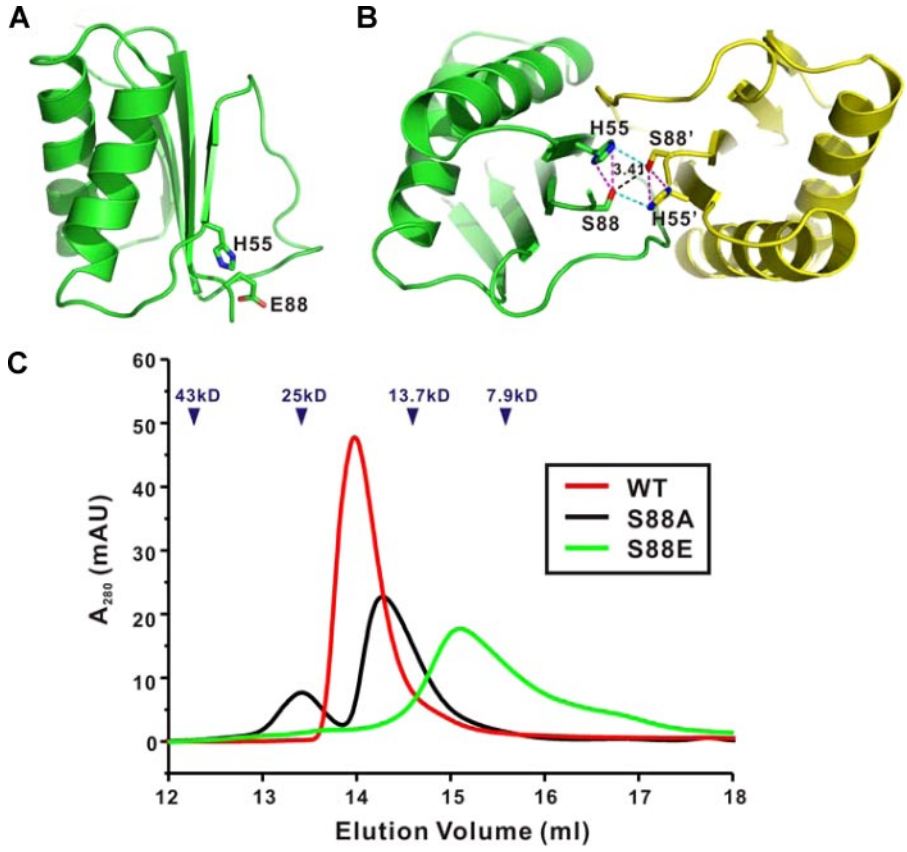

FIGURE 5. **Substitution of Ser[88] with Glu disrupts dimer formation of DLC1.** *A*, structure model of the S88E mutant of DLC8 using PDB code 1RHW. The structural model is built from the monomeric DLC1 structure determined at pH 3. The images were produced with PyMol (Delano Scientific LLC); residues His[55] and Ser[88]/Glu[88] are shown in the explicit atomic model. *B*, the ribbon diagram showing the His[55]–Ser[88] hydrogen bond network in the DLC1 dimer (PDB code 1F3C) interface. *C*, analytical gel filtration analysis of the wild-type DLC1, and its S88A and S88E mutants. The elution volumes of molecular mass standards are indicated at the *top* of the panel.

cytes at a faster rate. The differences in the extent of the mammary involution index among the various lines were quantified using the adipocyte percentages (Fig. 3*E*). Mammary glands from the MMTV-DLC1 mice had a similar percentage of adipocytes as those from the wild-type mice at all the time points examined. However, there was a significant increase in the proportion of adipose tissue in glands from the MMTV-DLC1-S88A mice compared with wild-type mice on involution days 3 and 4. These findings indicated that overexpression of wild-type DLC1 had no effect on mammary gland involution. In contrast, overexpression of DLC1-S88A accelerated mammary involution.

Consistent with this notion, we found an increase in the TUNEL-positive apoptotic cells in the mammary glands from the MMTV-DLC1-S88A mice compared with TUNEL-positive cells from the glands of the control mice (Fig. 4*A*). These observations suggested that S88A might accelerate involution by promoting apoptosis. Accordingly, there was an increase in the levels of phosphorylated STAT3-Tyr[705], a known involution-associated marker, on involution days 2 and 3 in the mammary glands from the MMTV-DLC1-S88A mice compared with age-matched control mice (Fig. 4*B*). Bcl-xL, an anti-apoptosis marker of mammary gland involution, was decreased in mammary glands from the MMTV-DLC1-S88A mice compared with age-matched control mice (Fig. 4*B*). There was no difference in the levels of the above markers between the MMTV-DLC1 and control non-transgenic mice (Fig. 4*B*).

We next tested the status of Bim in the mammary glands from age-matched non-transgenic, MMTV-DLC1, and MMTV-S88A mice using immunostaining and immunoblot assays. On day 2 involution, mammary glands from the non-transgenic and MMTV-DLC1 mice had barely detectable Bim, the MMTV-DLC1-S88A mammary glands showed a significant immunostaining of Bim, as shown by a brown color (Fig. 4*C*). By involution day 3, all of the glands showed a higher Bim level than on day 2, whereas mammary glands from the MMTV-S88A mice showed a much higher level (Fig. 4*C*). Sections from the same mammary gland were stained for T7 to show the transgene expression (supplementary Fig. S7). Immunoblot assay of mammary glands on involution day 3 also showed that MMTV-S88A glands had higher Bim than did control mouse glands (Fig. 4*D*). Taken together, these observations indicated that overexpression of a Ser[88] phosphorylation-inactive DLC1 (DLC1-S88A) caused apoptosis, probably due to increased levels of Bim.

Structural Basis and Implication of Ser[88] Phosphorylation—We next studied the structural consequence of Ser[88] phosphorylation on DLC1. DLC1 exists as a dimer at physiological pH and dissociates into a folded monomer at very low pH (<4.5) (38, 39). Ser[88] upon phosphorylation or substitution by glutamic acid is likely to be exposed in the non-steric hindrance area of the molecule. Interestingly, His[55], a site known to undergo protonation, comes in parallel with that of Ser[88] (Fig. 5*A*). Protonation of the buried His[55] is likely to be responsible for the pH-induced dimer-to-monomer transition of DLC1 (Ref. 39 and Fig. 5*B*). In the DLC1 dimer, His[55] from each monomer stacks against each other, and both His residues are completely buried in the dimer interface (Fig. 5*B*). However, the S88E mutant of DLC1 is deficient in binding to endogenous DLC1 under physiological pH (Fig. 1). A close-up view of the DLC1 dimer interface shows that the side chain of Ser[88] is also buried. The hydroxyl group of each Ser[88] has the potential to form hydrogen bonds with the imidazole rings of both His residues (His[55] and His[55′]). Thus, the resulting interaction between the two pairs of His[55]/Ser[88] in the hydrophobic dimer interface should play critical roles in the stability of the DLC1 dimer. Additionally, the distance between the two hydroxyl

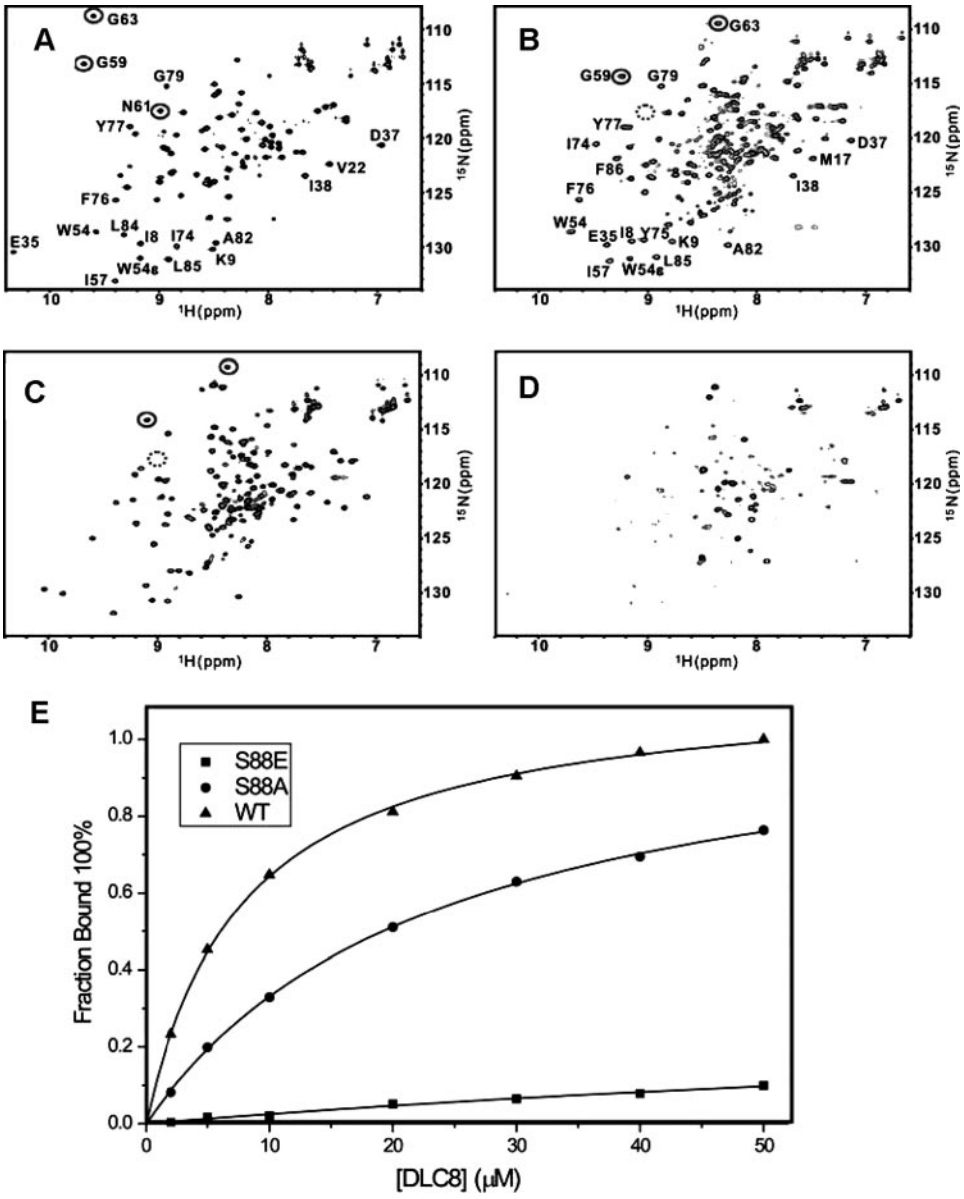

FIGURE 6. **The S88E mutant of DLC1 forms a stable monomer and is not capable of binding to its target Bim.** The figure shows the ^{1}H-^{15}N HSQC spectra of the wild-type DLC1 at pH 6.0 (*A*), WT DLC1 at pH 3.0 (*B*), the S88E mutant of DLC8 at pH 6.0 (*C*), and the S88A mutant at pH 6.0 (*D*). For clarity, only selected peaks are labeled with their assignment. The residues marked with *open ovals* in *A* are characteristic for the dimer conformation, and these peaks completely disappeared in the monomer forms of DLC1 in *panels B* and *C*. *E*, fluorescence polarization titration curves measuring the binding of the wild-type, S88A, and S88E forms of DLC1 with the Bim peptide.

groups of Ser[88] in the DLC1 dimer is 3.41 Å, a distance much too small to accommodate two bulky phosphate groups.

The above structural considerations in the context of our biologic data allowed us to predict that phosphorylation of Ser[88] in DLC1 will have a major effect on the packing and may potentially lead to the complete dissociation of the DLC1 dimer. To experimentally test this hypothesis, we pursued several approaches. First, we analyzed the molecular masses of the wild-type DLC1 and its S88E and S88A mutants using analytical gel filtration chromatography. The Ser[88] to Glu mutation mimicked Ser[88] phosphorylation. The Ser[88] to Ala substitution mimicked the non-phosphorylatable form of DLC1. As expected, the wild-type DLC1 was eluted at a volume suggestive of its being a dimer. In contrast, the DLC1-S88E mutant exhibited an elution profile consistent with being a pure monomer. The DLC1 S88A mutant was eluted with two peaks. The major peak was in the middle between the wild-type dimer and the S88E monomer, presumably due to intermediate exchange between dimer and monomer conformations of the mutant (Fig. 5*C*). This dynamic exchange is supported by the NMR spectrum of the S88A mutant shown in Fig. 6*D* (see below). The minor peak eluted at a molecular mass larger than the dimer peak of the wild-type protein, and this peak likely represents the higher order aggregation of the mutant.

To obtain definitive conformational status of the mutants, we resorted to NMR spectroscopic studies, as the ^{1}H-^{15}N HSQC spectrum is a very reliable indicator for monitoring dimer-to- monomer transition of DLC1 (38). The wild-type DLC1 adopts a stable dimer at pH 6.0, and the HSQC spectrum of the protein serves as the reference for the dimer conformation (Fig. 6*A*). When the pH of the wild-type protein is decreased to 3.0, the protein dissociates to a folded monomer, as expected from the previous studies (38). The HSQC spectrum of the wild-type DLC1 at pH 3.0 was used as the reference spectrum of the monomeric form of protein (Fig. 6*B*). The most characteristic changes in the HSQC spectra of DLC1 accompanying the dimer-to-monomer transition were large shifts of peaks connecting β1- and β2-strands (residues 59–63, highlighted with *open ovals* in Fig. 6*A*), as this region undergoes dramatic conformational changes upon dimer dissociation (38). The well dispersed HSQC spectrum of the S88E mutant of DLC1 at pH 6.0 indicated the mutant protein is folded, and the spectrum of the protein resembled that of the monomeric, wild-type protein at pH 3.0. For example, the two characteristic peaks, Gly[59] and Gly[63], both critical for the formation of the DLC1 dimer, shifted to the positions corresponding to the monomer conformation of the protein (Fig. 6, *B* and *C*). The HSQC spectrum of S88A was severely broadened (Fig. 6*D*), and this is consistent with the observation in the gel filtration chromatography that the protein is probably undergoing conformational exchange between monomer and dimer. Finally, we com-

pared the binding properties of the wild-type DLC1 and its mutants with a peptide encompassing the DLC1-binding domain of Bim by fluorescence spectroscopy. The wild-type DLC1 bound robustly to the Bim peptide, with a dissociation constant of 1.28 ± 0.05 μM. Substitution of Ser^{88} with Glu essentially disrupted the Bim peptide binding of DLC1, as the S88E DLC1 mutant had no detectable binding to the peptide (Fig. 6*E*). This finding is consistent with our earlier observation that formation of DLC1 dimer is obligatory for its target binding (38). Substitution of Ser^{88} with Ala led to a slight decrease of DLC1 in binding to the Bim peptide (K_d ~2.29 ± 0.10 μM). This quantitative Bim peptide binding data of S88A DLC1 explains why the introduction of this non-phosphorylatable mutant DLC1 into cells would result in constitutive sequestration of Bim. Taken together, our data from the gel filtration chromatography, NMR spectroscopy, and fluorescence spectroscopy studies indicated that substitution of Ser^{88} with phosphorylation-mimicking Glu leads to the dissociation of DLC1 from a stable dimer to a folded monomer, thereby releasing its substrate Bim from DLC1.

DLC1 has a diverse array of binding partners. The monomer form of DLC1 is incapable of binding to target proteins, and dimerization might strengthen the DLC1 interaction with its partner (26, 32, 38). Therefore, it has been suggested that the monomer-dimer equilibrium could play a regulatory role in the function of DLC1 (33). Previous *in vitro* studies using recombinant glutathione *S*-transferase proteins *in vitro* have shown that phosphorylated or S88E DLC1 did not interact with the Bim cargo, whereas the S88A mutant of DLC1 has no effect on its binding to Bim (34). However, in our current *in vivo* cellular study, we repeatedly observed that Bim-L binding to S88A DLC1 was reduced, although phosphorylated or S88E DLC1 did not dimerize with DLC1 or interact with the Bim-L. This discrepancy between results could be due to the use of two different models (*in vitro* and *in vivo*) to study DLC1/Bim-L binding in two different studies. In any case, because physiologically *in vivo* results represent a physiologic relevant situation, we believe that phosphorylation on serine 88 plays an important role in controlling the functions of DLC1, through interaction with its substrates. In this regard, it is interesting to note that a recent study by Mohan *et al.* (40) has shown that conformational dynamics can regulate target binding by the DLC8 dimer.

Conclusion—In conclusion, we discovered for the first time that serine 88 phosphorylation on DLC1 acts as a molecular switch that controls the DLC1 dimer-monomer transition, thereby modulating its interaction with substrates and consequently regulating the functions of DLC1. This conclusion is evidenced by the decreased ability of transiently transfected DLC1-S88E to interact with the endogenous DLC1 and to dimerize in immunoprecipitation assays. This was further supported by phosphorylation-mimicking mutation leading to dissociation of the DLC1 dimer to a pure folded monomer in gel filtration chromatography and NMR studies. Furthermore, our study indicated the functional consequence of the above regulatory mechanism using cellular and mouse mammary gland models. Together, our results provide a molecular mechanism for the role of DLC1 Ser^{88} phosphorylation in conferring a survival advantage by modulating the levels of DLC1-Bim (supplementary Fig. S8).

Acknowledgments—We thank Amjad H. Talukder for assistance in transgenic mice generation, Rozita Bagheri-Yarmand for help in the early phase of this work, and Rajesh Singh for assisting in the in silico analysis with the protein group.

REFERENCES

1. Oiwa, K., and Sakakibara, H. (2005) *Curr. Opin. Cell Biol.* **17,** 98–103
2. Vallee, R. B., and Sheetz, M. P. (1996) *Science* **271,** 1539–1544
3. Hirokawa, N., Noda, Y., and Okada, Y. (1998) *Curr. Opin. Cell Biol.* **10,** 60–73
4. Vale, R. D. (2003) *Cell* **112,** 467–480
5. Piperno, G., and Luck, D. J. (1979) *J. Biol. Chem.* **254,** 3084–3090
6. King, S. M., and Patel-King, R. S. (1995) *J. Biol. Chem.* **270,** 11445–11452
7. Jaffrey, S. R., and Snyder, S. H. (1996) *Science* **274,** 774–777
8. Crepieux, P., Kwon, H., Leclerc, N., Spencer, W., Richard, S., Lin, R., and Hiscott, J. (1997) *Mol. Cell. Biol.* **17,** 7375–7385
9. Lo, K. W., Kan, H. M., Chan, L. N., Xu, W. G., Wang, K. P., Wu, Z., Sheng, M., and Zhang, M. (2005) *J. Biol. Chem.* **280,** 8172–8179
10. Naisbitt, S., Valtschanoff, J., Allison, D. W., Sala, C., Kim, E., Craig, A. M., Weinberg, R. J., and Sheng, M. (2000) *J. Neurosci.* **20,** 4524–4534
11. Fuhrmann, J. C., Kins, S., Rostaing, P., El Far, O., Kirsch, J., Sheng, M., Triller, A., Betz, H., and Kneussel, M. (2002) *J. Neurosci.* **22,** 5393–5402
12. Puthalakath, H., Huang, D. C., O'Reilly, L. A., King, S. M., and Strasser, A. (1999) *Mol. Cell* **3,** 287–296
13. Schnorrer, F., Bohmann, K., and Nusslein-Volhard, C. (2000) *Nat. Cell Biol.* **2,** 185–190
14. Rayala, S. K., den Hollander, P., Balasenthil, S., Yang, Z., Broaddus, R. R., and Kumar, R. (2005) *EMBO Rep.* **6,** 538–544
15. Rayala, S. K., den Hollander, P., Manavathi, B., Talukder, A. H., Song, C., Peng, S., Barnekow, A., Kremerskothen, J., and Kumar, R. (2006) *J. Biol. Chem.* **281,** 19092–19099
16. Hollander, P., and Kumar, R. (2006) *Cancer Res.* **66,** 5941–5949
17. Jacob, Y., Badrane, H., Ceccaldi, P. E., and Tordo, N. (2000) *J. Virol.* **74,** 10217–10222
18. Raux, H., Flamand, A., and Blondel, D. (2000) *J. Virol.* **74,** 10212–10216
19. Epstein, E., Sela-Brown, A., Ringel, I., Kilav, R., King, S. M., Benashski, S. E., Yisraeli, J. K., Silver, J., and Naveh-Many, T. (2000) *J. Clin. Investig.* **105,** 505–512
20. Lo, K. W., Naisbitt, S., Fan, J. S., Sheng, M., and Zhang, M. (2001) *J. Biol. Chem.* **276,** 14059–14066
21. Navarro-Lerida, I., Martinez, M. M., Roncal, F., Gavilanes, F., Albar, J. P., and Rodriguez-Crespo, I. (2004) *Proteomics* **4,** 339–346
22. Beckwith, S. M., Roghi, C. H., Liu, B., and Ronald, M. N. (1998) *J. Cell Biol.* **143,** 1239–1247
23. Dick, T., Ray, K., Salz, H. K., and Chia, W. (1996) *Mol. Cell. Biol.* **16,** 1966–1977
24. Phillis, R., Statton, D., Caruccio, P., and Murphey, R. K. (1996) *Development* **122,** 2955–2963
25. Chang, Y. W., Jakobi, R., McGinty, A., Foschi, M., Dunn, M. J., and Sorokin, A. (2000) *Mol. Cell. Biol.* **20,** 8571–8579
26. Fan, J., Zhang, Q., Tochio, H., Li, M., and Zhang, M. (2001) *J. Mol. Biol.* **306,** 97–108
27. King, S. M., Barbarese, E., Dillman, J. F., III, Patel-King, R. S., Carson, J. H., and Pfister, K. K. (1996) *J. Biol. Chem.* **271,** 19358–19366
28. Nyarko, A., Hare, M., Hays, T. S., and Barbar, E. (2004) *Biochemistry* **43,** 15595–15603
29. Wang, L., Hare, M., Hays, T. S., and Barbar, E. (2004) *Biochemistry* **43,** 4611–4620
30. Rodriguez-Crespo, I., Yelamos, B., Roncal, F., Albar, J. P., Ortiz de Montellano, P. R., and Gavilanes, F. (2001) *FEBS Lett.* **503,** 135–141
31. Benashski, S. E., Harrison, A., Patel-King, R. S., and King, S. M. (1997) *J. Biol. Chem.* **272,** 20929–20935

32. Liang, J., Jaffrey, S. R., Guo, W., Snyder, S. H., and Clardy, J. (1999) *Nat. Struct. Biol.* **6,** 735–740
33. Nyarko, A., Cochrun, L., Norwood, S., Pursifull, N., Voth, A., and Barbar, E. (2005) *Biochemistry* **44,** 14248–14255
34. Vadlamudi, R. K., Bagheri-Yarmand, R., Yang, Z., Balasenthil, S., Nguyen, D., Sahin, A. A., den Hollander, P., and Kumar, R. (2004) *Cancer Cell* **5,** 575–585
35. Yang, Z., Vadlamudi, R. K., and Kumar, R. (2005) *J. Biol. Chem.* **280,** 654–659
36. Bokoch, G. M., Reilly, A. M., Daniels, R. H., King, C. C., Olivera, A., Spiegel, S., and Knaus, U. G. (1998) *J. Biol. Chem.* **273,** 8137–8144
37. Seol, M. B., Bong, J. J., and Baik, M. (2005) *Mol. Cell* **20,** 97–104
38. Wang, W., Lo, K. W., Kan, H. M., Fan, J. S., and Zhang, M. (2003) *J. Biol. Chem.* **278,** 41491–41499
39. Makokha, M., Huang, Y. J., Montelione, G., Edison, A. S., and Barbar, E. (2004) *Protein Sci.* **13,** 727–734
40. Krishna Mohan, P. M., and Hosur, R. V. (2007) *Biochem. Biophys. Res. Commun.* **355,** 950–955

Serine 88 Phosphorylation of the 8-kDa Dynein Light Chain 1 Is a Molecular Switch for Its Dimerization Status and Functions

Chunying Song, Wenyu Wen, Suresh K. Rayala, Mingzhi Chen, Jianpeng Ma, Mingjie Zhang and Rakesh Kumar

J. Biol. Chem. 2008, 283:4004-4013.
doi: 10.1074/jbc.M704512200 originally published online December 14, 2007

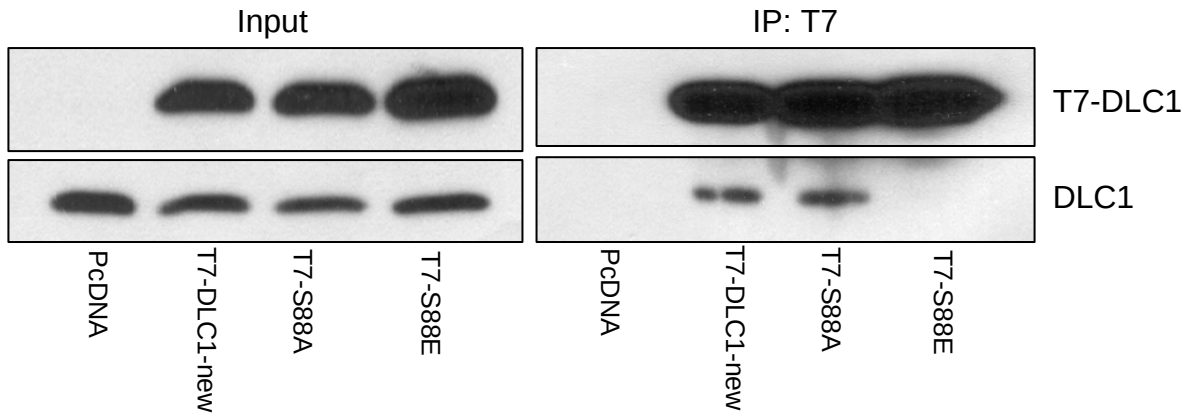

Fig S1. T7-DLC1-new interaction with endogenous DLC1. Total cellular lysates from 293T cells transfected with pcDNA, T7-tagged DLC1-new, S88A and S88E were immunoprecipitated with T7-antibody, followed by Western blot analysis for DLC1. The transiently expressed T7-DLC1-new protein showed the same ability to interact with endogenous DLC1 as did the T7-DLC1 used in Figure 1.

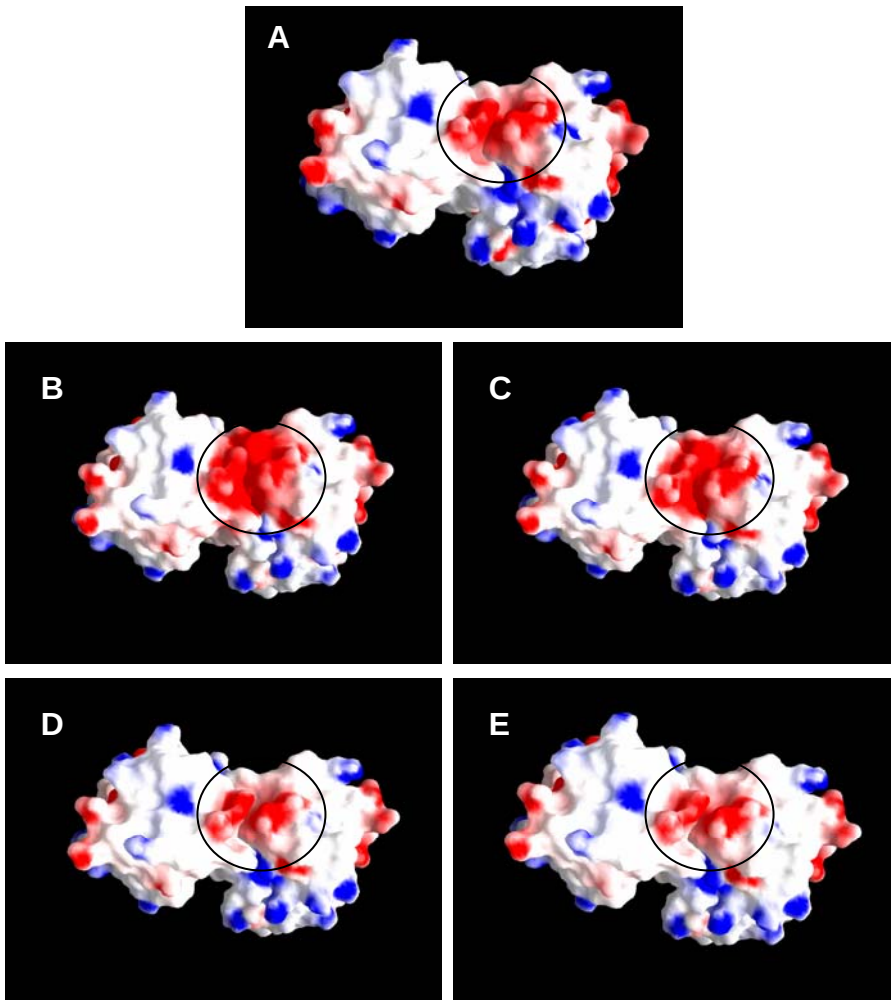

Fig. S2. Models showing the electrostatic surface diagrams of various combinations of DLC1 dimers. (A) Homodimer of DLC1-WT. (B) Homodimer of DLC1-WT with Serine-88 phosphorylate. (C) Homodimer of DLC1-S88E mutant. (D) Homodimer of DLC1-S88A mutant. (E) Heterodimer of DLC1-WT and DLC1 S88A mutant. Red and blue represent negative and positive electrostatic potentials, respectively, and areas of interest have been highlighted.

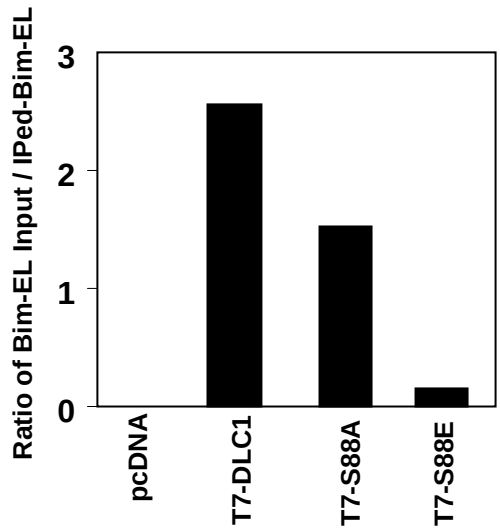

Fig. S3. Quantitation showing amount of Bim-EL binding to T7-DLC1, T7-S88A or T7-S88E in Figure 1A after normalization to the Bim-EL inputs. Quantification was performed by scanning both the immuoprecipitated Bim-EL and input Bim-EL bands, quantifying the band intensities using ImageQuant software and correcting for the unequal input Bim-EL bands.

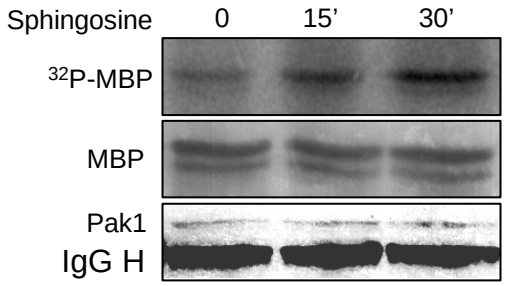

Fig. S4. Pak1 kinase assay in Figure 1B. Endogenous Pak1 was immunoprecipitated from the same lysates used in Figure 1B by Pak1 antibody. Ten micrograms of myelin basic protein (MBP) was used as a substrate for Pak1 kinase. IgG H: IgG heavy chain.

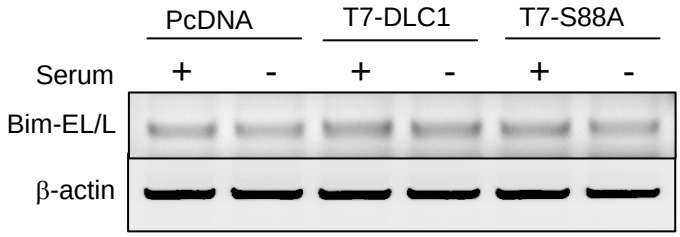

Fig. S5. RT-PCR analysis of Bim. Bim mRNA level of HC11/pcDNA, HC11/DLC1, and HC11/S88A cells growing in medium with or without serum for 24 hours. The RT-PCR primer used here can detect both Bim EL and Bim L. β-Actin was used as an internal control.

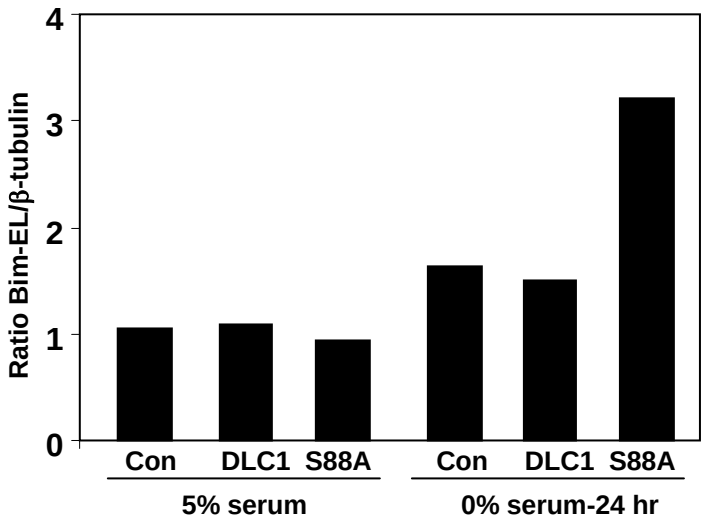

Fig. S6. Quantification showing the amount of Bim-EL increase in S88A clone after serum starvation. Quantification was performed by scanning both the Bim-EL and β-tubulin bands, quantifying the band intensities using ImageQuant software and correcting for the β-tubulin bands.

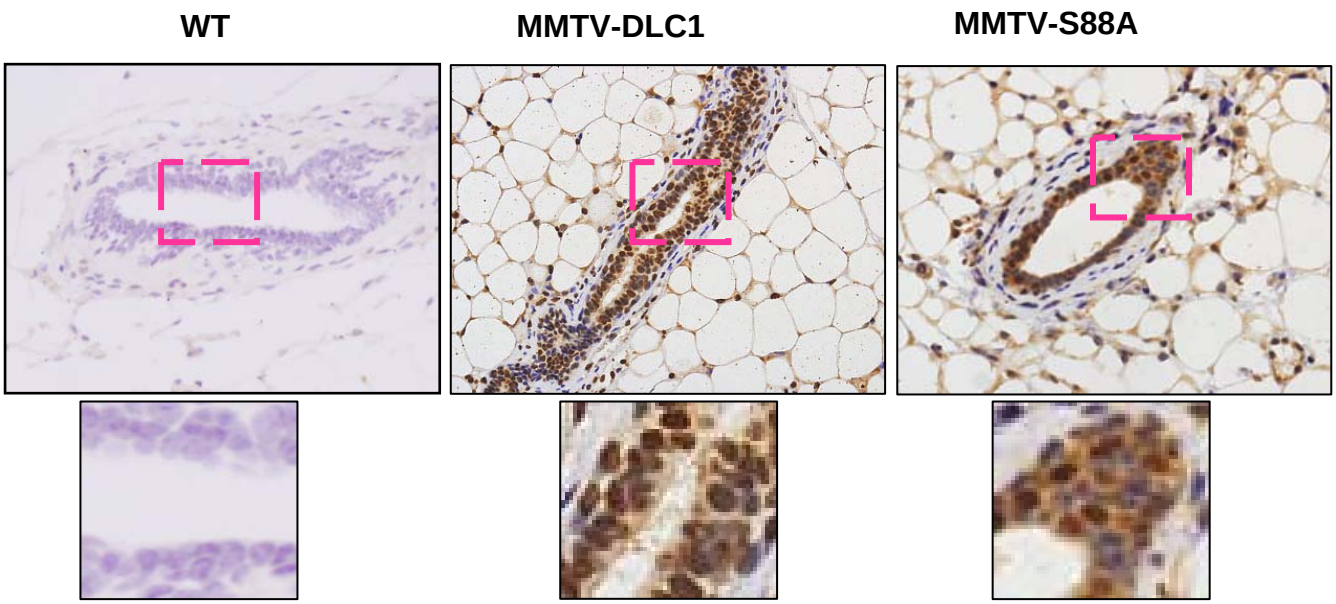

Fig. S7. Immunohistochemical analysis showing transgene expression in MMTV-DLC1 and MMTV-S88A mice. Mammary gland sections used in Fig. #4C from WT, MMTV-DLC1 and MMTV-S88A mice were stained for T7 expression to show the expression of the transgene. Images were enlarged to show clear staining of cells.

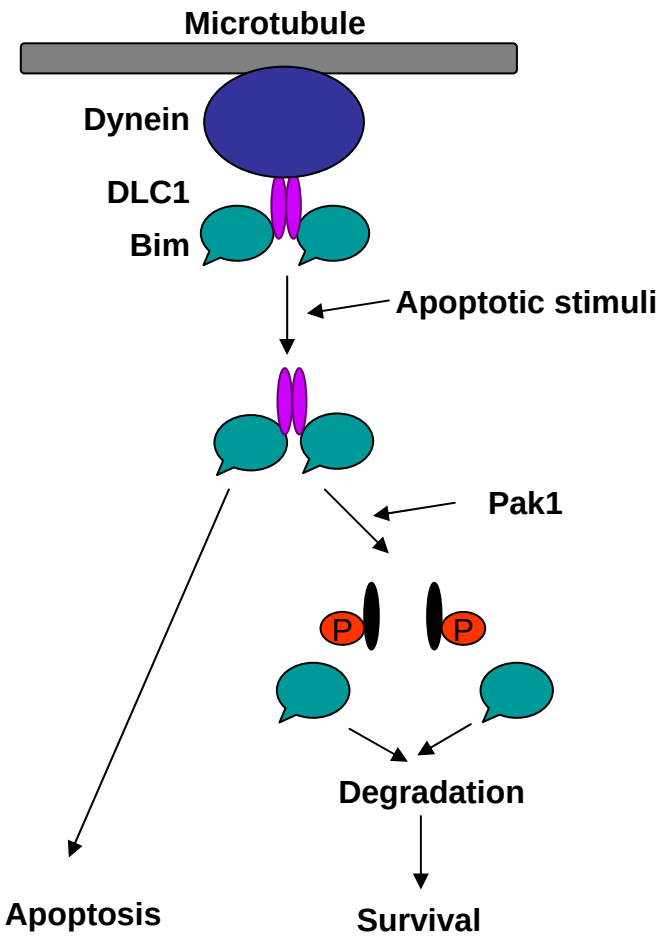

Fig. S8. Summary of the results presented in this article.